Photometric Mapping of Asteroid (4) Vesta from HST Observation. Jian-Yang Li[1], L.A. McFadden[1], P.C. Thomas[2], M. Mutchler[3], J.Wm. Parker[4], E.F. Young[4], C.T. Russell[5], M.V. Sykes[6], B. Schmidt[5], [1]Dept. of Astronomy, Univ. of Maryland, College Park, MD (*jyli@astro.umd.edu*), [2]Center for Radiophysics and Space Research, Cornell Univ., Ithaca, NY, [3]Space Telescope Science Institute, Baltimore, MD, [4]Southwest Research Institute, Boulder, CO, [5]IGPP, Univ. of California at Los Angeles, Los Angeles, CA, [6]Planetary Science Institute, Tucson, AZ.

Introduction: Asteroid (4) Vesta is the second most massive asteroid, and the only large asteroid known to have a basaltic surface that preserves a record of ancient volcanic activity. It is the first asteroid found to have similar spectrum with HED meteorites [1], and since considered to be the potential parent body. Later similar spectra of many small Vestoids (5-10 km size) whose orbits bridge Vesta's orbit and the 3:1 Kirkwood gap, where fragments can be delivered to Earth [2], were observed [3], stongly suggesting that HED meteorites originate from Vesta. The discovery of a huge crater on Vesta from HST observations in 1994 and 1996 [4] confirmed the existence of a collision that could excavate fragments from Vesta to form Vestoids and HED meteorites.

Previously Vesta was mapped by HST/WFPC2 in 1994, mainly covering the northern hemisphere from 15°S to 50°N latitude [5]. To better support NASA's Dawn spacecraft arriving at Vesta in 2011 [6], and to better study the huge crater which is near its south pole, we obtained WFPC2 images for the southern hemisphere of Vesta, at a sub-Earth latitude 18°S.

Observations and Data Reduction: Given the rotational period of Vesta ~5.423 hrs, and HST orbital period ~1.6 hr, we carefully planned the observation such that seven HST orbits were interleaved well yielding a complete and almost uniform coverage through all filters over the rotation of Vesta. Images were acquired with WFPC2 camera at a pixel scale of 38.5 km at Vesta, or about 9° longitude/latitude at disk center. The same four filters as previously used in 1994 and 1996 HST observations was used to facilitate directly comparisons. In addition, we obtained a few long exposures through wide R (F702W) filter for satellite search, which is reported elsewhere.

All raw images went through the standard HST calibration pipeline. We then performed the absolute photometric calibration using the standard photometric keywords PHOTFLAM and PHOTZPT to convert the images to intensity unit. Finally all images were converted to reflectance unit I/F, where I is the reflected intensity and πF is the incident solar flux integrated over the total bandpass of HST optical system for the corresponding filters. Further corrections for geometric distortion was unnecessary because 1) it is small for WFPC2, 2) Vesta is near the center of CCD chip, and 3) Vesta is only ~13 pixels across. CTE correction was skipped as well for reasons 2 and 3 above.

From these images the shape of Vesta was determined to agree with the previous shape model [7] very well, which will be used in our analysis.

Disk-integrated Lightcurves: The total brightness of Vesta was measured by integrating all pixels within an aperture. To correct for PSF, we measured the integrated brightness of Vesta through a series of apertures up until more than 50× the size of the PSF, and compared that with the encircled energy characteristics of the same apertures for the corresponding filter. Sky background is estimated negligible given the brightness of Vesta. Using phase correction 0.031 mag/deg, the rotational lightcurves through four filters were plotted in Fig. 1.

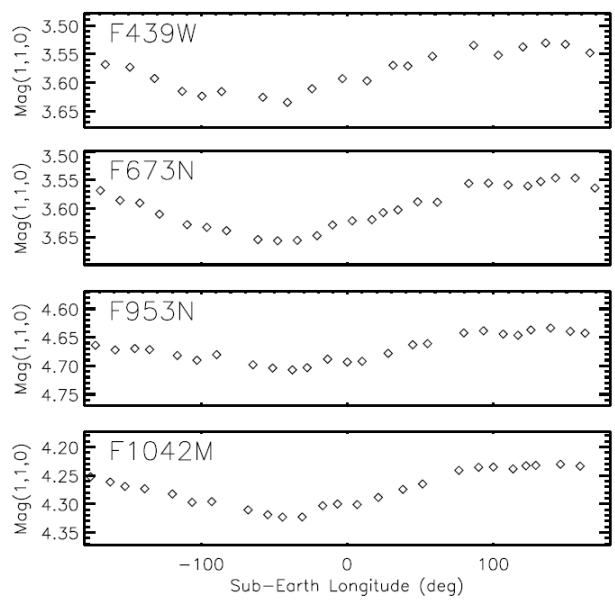

Fig. 1. Rotational lightcurves of Vesta plotted as a function of sub-Earth longitude in order to be compared with surface maps shown in Fig. 2 and 3. The uncertainties are dominated by PSF correction, and are 0.01 mag for F439W, F673N, and F953N filters, and 0.04 mag for F1042M filter.

Disk-resolved Photometry and Mapping: The disk-resolved photometric modeling and mapping is performed following the same method as used for Ceres mapping [8]. With images only at 8.5° and 9.5° phase angles, we assumed an asymmetry factor of the single-term Henyey-Greenstein single-particle phase function -0.3, an opposition amplitude 1.0, and an opposition width 0.04 [9]. The assumptions do not affect the mapping as limb profile is primarily determined by

roughness parameter (θ) and the single-scattering albedo (SSA). But the modeled SSA is affected. Disk-resolved Hapke modeling resulted in a θ of 50°-60°, which is not likely physical. This is likely due to the effect of PSF given the size of Vesta is only ~5 PSF. We then restored the images by Maximum Entropy Method for modeling and mapping. Photometric model is good only at incidence and emission angles smaller than 50°, limiting the final maps to be between latitudes 50°S to 20°N. The final modeled θ is ~30°, and the Minnaert k parameter is ~0.55.

After removing limb profiles from all images with the modeled globally averaged photometric parameters, they are projected onto the longitude-latitude coordinate of Vesta. The final maps were constructed by combining all projections. The maps from both original images and deconvolved images were compared and found consistent with each other, but the latter show obviously better results with less seams and artifacts. The final maps are in Fig. 2.

The maps in Fig. 2 and the lightcurves in Fig. 1 are consistent with each other even to the smallest scale features in the lightcurves. These maps overlap with the previous maps as reported in [5] between 15°S and 20°N latitudes, where they agree with each other. The western hemisphere is in general darker than the eastern hemisphere. The albedo near 1-μm band center is the most uniform over the surface compared with other wavelengths. The dark feature Olbers that has been used to define the Prime Meridian is the less visible at longer wavelengths. In western hemisphere just south to the equator (60°W, 10°S) is the darkest feature over the surface, showing some kind of tunneling at 20°S to Olbers. Another dark feature at eastern and southern hemisphere (100°E, 20°S), not shown in the previous maps, is visible in these maps. The brightest feature in the maps is near the lower edge at about (25°E, 40°S), and seems to be associated with the highest point on the rim of the south pole crater as shown in the topographic map reported in [4].

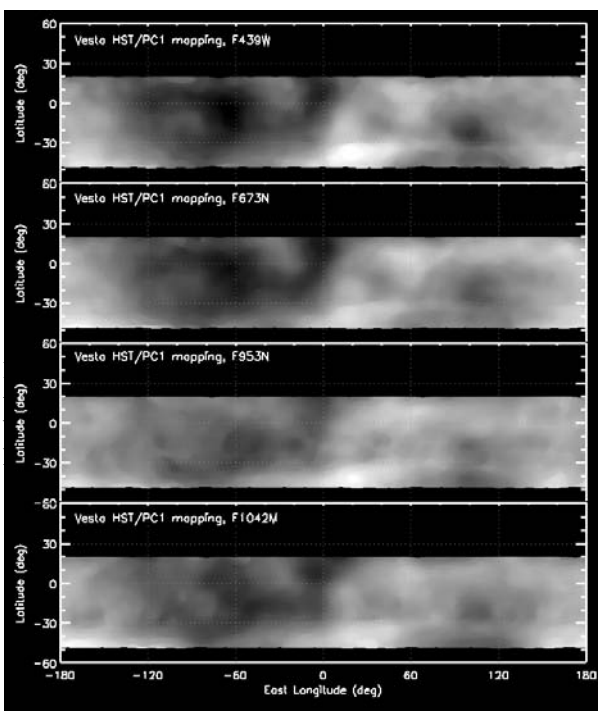

Fig. 2. Albedo maps of Vesta, displayed at a linear gray scale from -17% to +17% from their individual global averages for all four wavelengths. They are smoothed by 9° to match the original HST pixel scale.

Compositional Mapping: In order to extract compositional information of Vesta's surface, we combined the albedo maps at four wavelengths following the color scheme used in [5], as shown in Fig. 3, with the features identified in [5] marked.

Overall our map is consistent with the previous color composite map, and the mineralogical diversity is clearly shown. With more coverage to the south than the previous studies, we see broader and deeper 1-μm absorption that suggests more mixture with plutonic minerals near the rim and the central peak of the crater. This could be an indication of the excavation occurred during the formation of the crater. More work is needed to confirm it. Detailed studies on the shape of these features and the distribution of compositional minerals will uncover the formation of the crater, as well as that of Vestoids and HED meteorites.

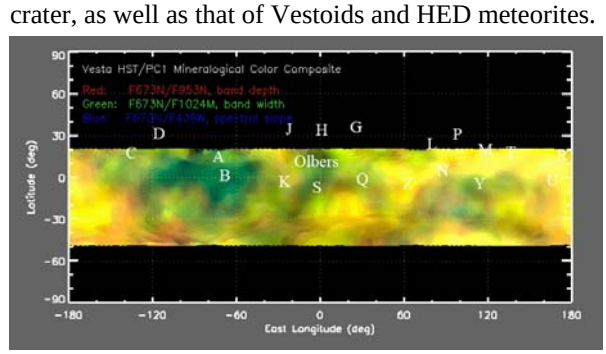

Fig. 3. Compositional map with the same color scheme as used in [5]. Red represents 1-μm band depth, green the band width, and blue the out-of-band red-slope. The color has been adjusted to match Fig. 3 in [5] as close as possible.

References: [1] McCord, T.B., Adams, J.B., and Johnson, T.V. (1970) *Science*, 168, 1445. [2] Wisdom, J. (1985) *Nature*, 315, 731. [3] Binzel, R.P., and Xu, S. (1993) *Science*, 260, 186. [4] Thomas, P.C. et al. (1997) *Science*, 277, 1492. [5] Binzel, R.P. et al. (1997) *Icarus*, 128, 95. [6] Russell, C.T. et al. (2007) *EM&P*, 101, 65. [7] Thomas et al. (1997) *Icarus*, 128, 88. [8] Li, J.-Y. et al. (2006) *Icarus*, 182, 143. [9] Helfenstein, P., and Veverka, J. (1989) *Asteroids II*, 557.